

Article

Estimating Rooftop Areas of Poultry Houses Using UAV and Satellite Images

A. Bulent Koc ^{1,*} , Patrick T. Anderson ¹, John P. Chastain ¹ and Christopher Post ²

¹ Department of Agricultural Sciences, Clemson University, Clemson, SC 29634, USA; ptander@clemson.edu (P.T.A.); jchstn@clemson.edu (J.P.C.)

² Department of Forestry and Environmental Conservation, Clemson University, Clemson, SC 29634, USA; cpost@exchange.clemson.edu

* Correspondence: bulent@clemson.edu

Received: 10 November 2020; Accepted: 7 December 2020; Published: 9 December 2020



Abstract: Poultry production requires electricity for optimal climate control throughout the year. Demand for electricity in poultry production peaks during summer months when solar irradiation is also high. Installing solar photovoltaic (PV) panels on the rooftops of poultry houses has potential for reducing the energy costs by reducing the electricity demand charges of utility companies. The objective of this research was to estimate the rooftop areas of poultry houses for possible PV installation using aerial images acquired with a commercially available low-cost unmanned aerial vehicle (UAV). Overhead images of 31 broiler houses were captured with a UAV to assess their potential for solar energy applications. Building plan dimensions were acquired and building heights were independently measured manually. Images were captured by flying the UAV in a double grid flight path at a 69-m altitude using an onboard 4K camera at an angle of -80° from the horizon with 70% and 80% overlaps. The captured images were processed using Agisoft Photoscan Professional photogrammetry software. Orthophotos of the study areas were generated from the acquired 3D image sequences using structure from motion (SfM) techniques. Building rooftop overhang obscured building footprint in aerial imagery. To accurately measure building dimensions, 0.91 m was subtracted from building roof width and 0.61 m was subtracted from roof length based on blueprint dimensions of the poultry houses. The actual building widths and lengths ranged from 10.8 to 184.0 m and the mean measurement error using the UAV-derived orthophotos was 0.69% for all planar dimensions. The average error for building length was 1.66 ± 0.48 m and the average error for widths was 0.047 ± 0.13 m. Building sidewall, side entrance and peak heights ranged from 1.9 to 5.6 m and the mean error was 0.06 ± 0.04 m or 1.2%. When compared to the horizontal accuracy of the same building measurements taken from readily available satellite imagery, the mean error in satellite images was -0.36% . The average length error was -0.46 ± 0.49 m and -0.44 ± 0.14 m for building widths. The satellite orthomosaics were more accurate for length estimations and the UAV orthomosaics were more accurate for width estimations. This disparity was likely due to the flight altitude, camera field of view, and building shape. The results proved that a low-cost UAV and photogrammetric SfM can be used to create digital surface models and orthomosaics of poultry houses without the need for survey-grade equipment or ground control points.

Keywords: photogrammetry; satellite; agriculture; ground sample distance; solar energy

1. Introduction

Poultry production is dependent on climate-controlled buildings that require large ventilation loads. For example, energy use data taken from seven broiler farms in South Carolina between 2003 and 2007 demonstrated an average annual electrical use of 2504 kWh per 100 m²/year, with a range of

1714 to 3598 kWh per 100 m²/year [1]. A typical broiler house with a floor area of 2322 m² required approximately 45,072 kWh/year [1]. Furthermore, electricity cost, on average, was over 50% of the annual energy cost, which included the use of liquefied petroleum gas (LPG) or natural gas in the winter season [1].

Installing solar photovoltaic (PV) panels on the rooftops of poultry houses has potential for reducing the energy costs of poultry production by producing own electricity and reducing the demand charges of utility companies. Poultry farms are usually located in rural areas with a low population density, far from centralized electric power production, and, in some cases, are remote from main transmission lines. Poultry farms are also spatially confined to approximately an 80-km radius from their contracted integrator company. Broiler farms are cleared of vegetation, making them ideal for PV device installation relative to most residential and urban buildings. Additionally, the National Poultry Technology Center concluded that the size and weight of rooftop PV panels posed no threat to the structural integrity of a poultry house [2].

For energy suppliers, the challenge of peak demand is caused by solar energy. As solar energy increases for a given region, so does ambient temperature, causing increased air conditioning demand in response. Solar irradiance is also fuel for electricity generation by a PV installation. The additional solar gain can produce additional PV electric output directly, which coincides with increased electric loads for climate control. Therefore, with PV technology, a potential exists for solar irradiance, which contribute to the summer peak demand problem may be part of the solution. Furthermore, an important facet of power supply in the summer is managing fuel input to the generating equipment to meet increased demand throughout the day. In the case of PV plants, the increase in solar energy throughout a given day occurs naturally without human oversight. This would function as automated fuel management for a PV peaking plant based on local solar irradiance and cloud cover. Other potential benefits for an energy supplier using rural poultry houses for PV installations include utilization of pre-existing land and distribution infrastructure, as well as in-house resources for electricians and permitting. A mutually beneficial partnership between the utility and their agricultural customers would even allow greater flexibility in initial project scope and assist in accelerating economic development for the surrounding community.

Assessment of rooftop suitability for solar irradiance is the number one criterion for PV installation [3]. As poultry houses are established in various sizes and orientations, their rooftops' suitability for PV installation need to be analyzed to determine solar irradiance to estimate the solar energy potential of poultry houses. Geographic Information System (GIS) data, such as orthophotos, and digital surface models (DSM) are essential to the design, execution, and monitoring of projects across disciplines, such as agriculture, architecture, engineering, energy, mapping, transportation, and surveillance. There are multiple techniques currently employed to obtain GIS data. Traditional methods include manned airborne sensors, such as Light Detection and Ranging (LiDAR) or photogrammetric cameras, manned ground methods, such as terrestrial laser scanning, or readily available satellite imagery from Earth-orbiting satellites.

LiDAR systems are used to assess the solar potential of rooftops based on surface topography, long-term direct and diffuse radiation, and shadowing effects [3]. A LiDAR sensor which can be mounted on manned or unmanned aerial vehicle emits pulsed light waves in the range of 10- to 250-nm wavelengths into surrounding environment. The pulsed light waves bounce off the surrounding objects and return to the sensor. The time it takes for the light wave to travel the distance between the sensor and the object and return to the sensor is used to calculate the distances the light travels. With laser scanning, millions of data points are generated to obtain a 3D point cloud. Using the point cloud data, the planes of the rooftops in 3D can be reconstructed automatically [3]. Levinson et al. [4] developed digital elevation models of trees and buildings using LiDAR to assess the solar access of residential buildings. Verso et al. [5] developed a model based on LiDAR data in a GIS software to calculate the best area for installing PV panels in urban environments. Another study conducted by

Wiginton et al. [6] used GIS and object-specific image recognition to determine the available rooftop area for PV installation.

Solar potentials of roof segments from publicly available solar irradiance data and satellite images of roofs were determined using a deep learning-based program called DeepRoof [7]. The researchers compared their model estimations with a LiDAR-based approach and found that DeepRoof accurately estimated the roof geometry (i.e., roof's orientation and pitch) for solar potential with 91.1% accuracy. The developed model assumes the satellite images of roofs are available. In another study, surveyors were trained to use GIS tools and simulation software to determine suitability of rooftops for PV installation by Kuthanazhi et al. [8]. They verified their GIS data with randomly selected site visits [8].

Satellites and manned airborne platforms offer spatial coverage at a landscape scale. Using a manned aerial vehicle platform would be quite expensive [9] and satellite images may provide poor spatial resolution at large cartographic scales, both of which would pose some limitations in estimating the solar potential of rooftops. Terrestrial survey equipment is expensive and time-consuming [10]. High-resolution photogrammetric point clouds obtained from small UAVs would be an alternative approach for estimating the solar potential of poultry house rooftops [11]. The onboard inertial measurement unit (IMU) and GPS without Ground Control Points (GCPs) were used to locate and orient images captured with a UAV [12]. Currently, the combination of structure from motion (SfM) photogrammetry and flexible UAV photogrammetry has the potential to produce a unique surface reconstruction tool, delivering orthophotos and DSMs with ground sample distance (GSD) or pixel size of 1.5 cm [13].

Data collection with UAVs is now increasingly adopted directly by researchers of many disciplines [14]. A study conducted in 2012 compared a UAV's consumer-grade digital camera with a survey-grade terrestrial laser scanner to demonstrate the 0.10 m vertical accuracy achieved using SfM with complex topography and complex land covers for geoscience applications [15]. Another recent study done in a highly variable and vegetated terrain with low-cost UAVs demonstrated that the standard deviation of digital elevation model (DEM) data with and without GCPs only differed by 0.06 m [16].

To determine if poultry farms could function as rurally distributed, peak-demand photovoltaic (PV) power plants to sparsely populated areas, this study explored the use of a low-cost UAV for 3D mapping applications in the context of large-scale rural environments (2.5 ha) to produce accurate spatial data without expensive onboard GPS or Real-Time Kinematic (RTK) hardware, terrestrial survey equipment, and without the use of GCPs in the field. This was accomplished by a statistical error analysis of digital orthophotos produced from UAV-based photogrammetric point clouds. The objective of this research was to investigate whether aerial images captured with a low-cost UAV can be used as an alternative to relatively high-cost LiDAR sensors or readily available satellite imagery for estimating the dimensions of rooftops of poultry houses in planning PV installation.

2. Materials and Methods

A total of 31 farms with 139 poultry houses were visited in Anderson and Oconee Counties in upstate South Carolina. The dimensional accuracies of specific building characteristics were compared in the orthophotos generated from satellite and UAV imagery. The dimensions of each poultry house's length (L), width (W), sidewall height (Hs), peak height (Hp), and side entrance ride height (Hr) were obtained from building blueprints and manual measurements and estimated from orthophotos generated from UAV and satellite imagery. Data collection for the building dimensions entailed a combination of remote sensing techniques validated by physical measurements as benchmarks. The horizontal building estimations from UAV images were compared to estimations from satellite images.

2.1. UAV Flights for Data Collection

The remote data collecting equipment was a DJI Mavic Pro UAV with an onboard digital camera. A flight planner application, Pix4D Capture, was utilized for each flight. This mobile application automated each flight to improve the results, safety, and efficiency of the data collection process. A double-grid flight pattern at an altitude of 69 m was used for the aerial surveys. The angle of the UAV camera during flight was set to capture images at an angle of -80° from the horizon. The camera was programmed to capture 80% frontal overlap of image content between consecutive pictures along the flight path and 70% side overlap between images from adjacent flight paths at ground level [17]. Overlap ensured sufficient subject redundancy captured between photos which improved the quality of 3D digital surface model reconstruction using photogrammetry. An illustration of the flight path is given in Figure 1. All equipment, calibrations, and parameters were held constant throughout the data collection process to minimize inflation in the variance of the response and bias in the estimation of the treatment mean.



Figure 1. Sample image of the unmanned aerial vehicle (UAV) flight path in Pix4D Capture.

The building rooftop lengths (L_i) and widths (W_i) including the overhang were measured from the aerial images using the Ruler tool [18] on each farm's orthomosaics image and they were adjusted to blueprint dimensions. Poultry building vertical measurements consisted of sidewall heights, peak heights, and side entrance ridge heights. These measurements were obtained using the Ruler tool [18] on each farm's DSM.

The producers provided building length and width measurements for the farms visited from building blueprints. Building width and length on a single building at each of the 31 visited farms were measured manually. These dimensions are illustrated in Figure 2. Building blueprint dimensions were provided in imperial units (ft) and converted to metric (m) units. These converted units were used as the measured building dimensions for comparison to UAV and satellite estimations. To account for overhang, an estimated value based on observations made on many poultry houses was subtracted from the overall building roof lengths and widths that were seen in the images. Based on the observations, it was determined that the typical overhang added 0.9144 m to the width and 0.6096 m to the length of

the building floorplan. The building width W_i (m) and length L_i (m) including overhang observed in the overhead images were adjusted to the floorplan width W (m) and length L (m) as follows:

$$W = W_i - 0.9144 \quad (1)$$

$$L = L_i - 0.6096 \quad (2)$$



Figure 2. Poultry house viewed from above, illustrating length (L) and width (W) estimations observed from UAV images.

Poultry building height measurements were taken to compare vertical dimensions using a UAV flight path and to ensure precise and accurate model reconstruction in the vertical plane. These were also used to determine building roof slope. A range of sidewall heights (H_s), peak heights (H_p), and side entrance ridge heights (H_r) were measured to provide a greater range of vertical heights to compare with measurements from UAV images. The building side entrance can be seen in the center of the buildings shown in Figure 2. All building heights were measured with a commercially available measuring tape (± 0.16 cm) (Komelon USD Division, Waukesha, WI), from the concrete base to under the building eave. The location of the sidewall and peak height measurements along with the location of building overhangs are illustrated in Figure 3.



Figure 3. Poultry end wall illustrating the location of sidewall and peak height measurements and building overhangs.

The amount of solar radiation that falls on roof-mounted solar PV panels depends on the rooftop azimuth and the slope of the southward-facing roof. Consequently, rooftop slope was needed for the current application of UAV and satellite remote sensing to evaluate the suitability of the poultry buildings for solar electric production. Slope was calculated using hand measurements or measurements from UAV images following the definition of roof slope (S) as:

$$S = (H_p - H_s)/(W \div 2) \quad (3)$$

2.2. UAV Image Data Processing

The computing equipment used for data processing was an iMac Desktop with a 4.2 gigahertz quad core i7 processor and 32 GB 2400 MHz Double Data Rate (DDR) Random Access Memory (RAM). The aerial photos were processed using Agisoft Photoscan Professional software [18] version 1.4.1 to construct 3D models. This processing involved examining relative, absolute, internal, and external orientations and the reconstruction of 3D models from the 2D captured images using the SfM photogrammetric range imaging technique [15,19]. The workflow consisted of 6 steps: (1) import and (2) align photos, (3) optimize alignment, (4) build dense point cloud, (5) build digital surface model, and (6) build orthomosaics image. The general process was to align images by matching common points, which resulted in a sparse point cloud and established camera positions. Next, a dense point cloud of improved accuracy was constructed based on the estimated camera positions and images. The maximum allowable number of points on every image available for consideration was 40,000 points, and the upper limit of points allowed to match between any two images was set to 10,000,000 points. These constraints allowed for optimization of the alignment process without allowing features to be overlooked. Adaptive camera model fitting was enabled, which automated the selection of camera parameters to be adjusted based on their reliability estimates. The dense point cloud was constructed using 4× downscaled images, which maintained a relatively high accuracy (compared to 16× or 64× downscaling). A mild depth filter was also applied during this step to remove outliers and noise.

2.3. Satellite Images

The poultry building lengths and widths of 139 buildings in 31 farms were also measured using readily available satellite imagery provided by Google, Maxar Technologies, and US Geological Survey [20]. The collective 139 building rooftop lengths (L_i) and widths (W_i) were measured using the Measure Distance tool [20] on satellite imagery of the 31 farms. Adjusted building width (W) and length (L) measurements from satellite imagery were obtained in the same way as for UAV-generated images using Equations (1) and (2). It was not possible to determine building heights from satellite images.

2.4. Comparison of Actual Building Dimensions Using UAV and Satellite Images

The predictive accuracy of building measurements within the satellite and UAV-derived orthoimages were determined using Equation (4):

$$\Delta d = A - M \quad (4)$$

where

Δd = difference between the actual dimension and the measured dimension (m);

A = actual dimension (m);

M = measured dimension (m).

Accuracy was measured by quantifying error as the difference between actual building dimensions observed and the dimensions measured from remote sensing-derived digital orthomosaics. This was done for building length (L), width (W), building sidewall height (H_s), peak height (H_p), and side entrance height (H_r). The actual dimensions were the blueprint dimensions for building length and

width and hand measurements of building heights. The measured dimensions were the estimated building measurements in the UAV- and satellite-derived orthomosaics images.

The smallest horizontal dimension that was measured for the poultry buildings was the building width and was in the order of 10 m. A UAV landing pad with a 0.75-m diameter was used to provide a smaller horizontal dimension to test the accuracy of using UAV-captured images for making horizontal landscape measurements. The UAV landing pad was visible in each flight and was used as a reference point to ensure precise and accurate large-scale horizontal model reconstruction. The pad was made of waterproof, high-quality nylon stretched between a circular steel ring frame. The ring was manufactured to be flexible for contorted compaction to facilitate storage and transportation. This lack of rigidity also allowed for potential variation in pad diameter measurements. The round pad diameter was hand-measured 9 times to the nearest 0.16 cm with the measuring tape. The average of these measurements was the actual landing pad diameter. The landing pad diameter was also measured using the computer software's orthomosaic images once per flight to provide 31 observations. The mean landing pad diameter obtained by hand measurements was compared to the mean pad diameter measured using UAV images by calculating the 95% confidence interval (C.I.) about each mean as [21]:

$$\text{C.I.} = t_{\alpha, (n-1)} \times (s/n^{0.5}) \quad (5)$$

where

C.I. = 95% confidence interval about the mean (m);

t = t -value $_{0.025, (n-1)}$;

s = standard deviation (m);

n = number of replications.

The mean difference (Δd) was calculated for the building lengths (L) and widths (W) measured using both the UAV and satellite images as well as the sidewall (H_s), peak (H_p), and side entrance heights (H_r) measured using only the UAV images. The mean differences were compared using the 95% confidence interval about the means, as shown in Equation (5). Relative error was also calculated for differences for all building length, width, and height dimensions obtained using both UAV and satellite images using Equation (6). This was done to place the error in perspective of the size of the measurements.

$$\mu E = (\mu \Delta d / \mu A) \times 100 \quad (6)$$

where

μE = mean error (%);

$\mu \Delta d$ = mean difference (m);

μA = mean actual dimension (m).

The percent error was calculated as the mean of all calculated differences for a specific building dimension divided by the grand mean of all actual measurements of a specific dimension. This metric established measured error relative to the size of the measurement, which was useful due to the variation in measurements ranging from a UAV landing pad with a diameter of less than one meter to a building with a length greater than 150 m.

It was hypothesized that the variances in ΔW and ΔL obtained based on UAV and satellite remote sensing would not be the same. To test this hypothesis, an F-test for common variance was used to determine if results could be pooled. The calculated F was determined by dividing the largest variance of one horizontal dimension (ΔW or ΔL) by the smaller variance of the other horizontal dimension (ΔW or ΔL), each from the same remote sensing tool [21]. The calculated F was compared with the tabulated F using the degrees of freedom for the numerator and denominator at the 95% level of probability. If the F-test indicated that the variances were not significantly different, then the variances would be pooled to provide a better estimate of the variance used for calculation of the 95% C.I.

Finally, the raw data for all heights, widths, and lengths for the UAV image-derived measurements were correlated with the actual measurements using a line equation that passed through the origin.

This was done to allow visualization of the raw data (a check of correlation of the data) and to provide an overall estimate of the average difference between the actual dimensions and the UAV-derived measurements. A similar correlation was done for the widths and lengths obtained from the satellite image measurements as well.

3. Results and Discussion

The products of all methods described for remotely sensed data collection, photogrammetric data processing, and statistical analysis are given below. Dimensional accuracy was compared for horizontal measurements of the UAV landing pad and poultry house building dimensions, and then vertical measurements of the building sidewall and peak heights. These numbers were compared to the accuracy of horizontal measurements from satellite images. The image quality was critical for the successful adaptation of that tool. In addition, the camera's ability to capture the details of environments that contain complex topography and complex land cover would also improve its usefulness. The quality of an image captured with the UAV camera is shown in Figure 4. This image depicts a portion of a poultry barn and the surrounding rural landscape.



Figure 4. Sample image of a poultry house rooftop captured with the UAV at a 69-m altitude.

Sample image EXIF data associated with Figure 4 are given in Table 1. Exchangeable Image File Format (EXIF) is a standard that defines specific information related to an image or other media captured by a digital camera [22].

EXIF data included camera exposure, GPS location, and date/time of the image captured. This information was critical for understanding the operational parameters (such as aperture, shutter speed, and exposure) and equipment limitations (image size or focal length) of the tools utilized during data collection.

The focal length of the camera was 4.7 mm. Digital zoom was 0. The image size was 4k pixels in length by 3k pixels in width. These details, among others included in the Table 1, such as exposure and zoom, are useful for validating remote sensing equipment. This information is also vital for calculating ground sampling distance (GSD, cm/pixel) for relative accuracy of images.

Table 1. Sample UAV image Exchangeable Image File Format (EXIF) information.

Aperture Value:	2.27
Color Space:	sRGB
Components Configuration:	0,3,2,1
Compressed Bits per Pixel:	2.897
Contrast:	Normal
Custom Rendered:	Normal Process
Digital Zoom Ratio:	0
EXIF Version:	2.3
Exposure Bias Value:	0
Exposure Index:	0
Exposure Mode:	Auto Exposure
Exposure Program:	Normal Program
Exposure Time:	1/60 s
File Source:	DSC
Flash:	No Flash Function
FlashPix Version:	0.1
FNumber:	2.2
Focal Length:	4.7 mm
Focal Length in 35mm Film:	26 mm
Gain Control:	None
Photographic Sensitivity (ISA):	147
Light Source:	Unknown
Max Aperture Value:	2.27
Metering Mode:	Center Weighted Average
Pixel X Dimension:	4000
Pixel Y Dimension:	3000
Saturation:	Normal
Scene Capture Type:	Standard
Sharpness:	Normal
Shutter Speed:	1/60 s
White Balance:	Auto white balance

3.1. UAV Remote Sensing and Photogrammetry

The results for UAV flight logistics included the flight time at each farm and the total number of images captured by the UAV. The software processing of these images resulted in filtering images, identifying tie points between images, and construction of a dense point cloud. A summary of these results for the entire project as well as an estimated average per farm are given in Table 2.

Table 2. Summary of data collection and processing results.

	Average/Farm	Project Total
Flight Time (min)	13.5	320
Images Captured	268	8043
Images Used	224	6836
Tie points Identified	666,691	20,000,715
Dense Cloud Points	54,209,477	1,626,284,298

The average flight path aerial grid size was 28,525 m² (175 m × 163 m). The average number of images captured at each farm was 268. Eighty-five percent of the images were utilized by the software. This means that 15% of captured images were deemed to be of unsuitable quality to benefit the analysis and were automatically excluded by the software in steps 1 and 2 of the photogrammetry workflows. A total of 6836 images were used, from which a collective 20 million tie points were identified with the reconstruction parameters. The project study area had a total of 1.63 billion 3D dense cloud points. The results for a reconstructed key point cloud can be seen in Figure 5a and a dense point cloud output can be seen in Figure 5b. The general process was to align images by matching common points,

which resulted in a sparse point cloud and established camera positions. Then, a dense point cloud of improved accuracy was constructed based on the estimated camera positions and pictures.

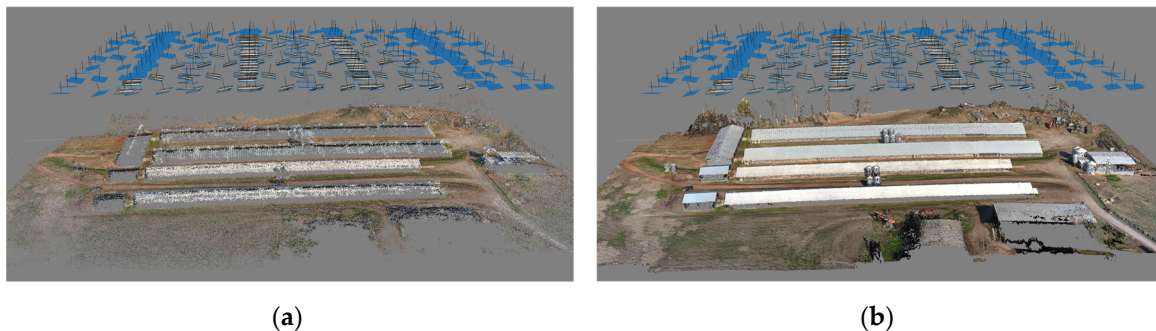


Figure 5. Farm buildings reconstructed in Photoscan Pro as (a) a sparse 3D point cloud of 650,956 points, and (b) a dense 3D point cloud of 46,764,137 points with camera locations and thumbnails above.

The goal of the data collection and analysis was the creation of a digital orthomosaic image as well as a DSM for future solar analysis. The orthomosaic (similar to the digital product provided in satellite imagery) was used to predict building dimensions. The image clarity and resolution of each image, as well as maximizing the tie points between images, were critical for accurate renderings of the subject area. For this study, this affected the confidence of agricultural building dimension measurements. The digital orthomosaic provided an aerial perspective, while the DSM provided surface texture and depth for the subject area. An example digital orthomosaic is shown in Figure 6a and a DSM of a surveyed farm is shown in Figure 6b.



Figure 6. (a) Orthomosaic image ($14,335 \times 11,647$, 1.93 cm/px) and (b) digital surface model (DSM) (9548×7884 , 3.86 cm/px) built from dense point cloud (DPC).

3.2. Statistical Analysis and Comparison of Actual and Measured Dimensions

3.2.1. Measured Error from UAV

The horizontal difference analysis was broken into two relative groups: cartographic small scale and large scale. The UAV landing pad functioned as the large-scale horizontal difference analysis, and the poultry house building length and width dimensions functioned as the small-scale horizontal difference analysis. The poultry house building side wall, side entrance, and peak height measurements were used for the vertical difference analysis. The round landing pad was hand-measured nine times in the field. The relatively small number of control trials was due to a low uncertainty associated with the simple hand measurements. The landing pad diameter was also determined within the computer software orthomosaic image 31 times. The results of the calculated differences between actual (hand) and predicted (UAV) measurements of the landing pad diameter are summarized in

Table 3. This includes the mean error (Equation (4)), standard deviation, 95% C.I. (Equation (5)), and percent error (Equation (6)).

Table 3. Comparison of UAV landing pad diameter measurements.

	Hand	Software
n =	9	31
Mean Pad Diameter (cm)	74.5	74.62
Standard Deviation, s (cm)	0.111	1.120
$t_{0.025, (n-1)}$	2.306	2.042
Standard error (cm)	0.037	0.201
95% Confidence Interval (cm)	± 0.085	± 0.412

The average hand measurement in the field was 74.5 cm, with a standard deviation of 0.111 cm. The field measurements had a 95% C.I. of ± 0.085 cm (74.42 cm, 74.59 cm). The landing pad diameter was measured within the computer software orthomosaic image 31 times, which was reflective of the number of flight trials. The average software pad diameter measurement was 74.62 cm, with a standard deviation of 1.120 cm. The software model had a 95% C.I. of ± 0.412 cm (74.21 cm, 75.03 cm). The computed difference between the means was 0.12 cm (0.16%). The results show that there was no significant difference between the mean pad diameter measured by hand and software at the 95% level [21].

Poultry house building length (L) and width (W) were each measured with plan dimensions obtained from the grower for 31 buildings, once at each farm. This was reflective of the number of flight trials. Length (L_i) and width (W_i) were also measured within the UAV-derived orthomosaic images 31 times and adjusted to account for rooftop overhang. A regression analysis of the horizontal building dimensions between blueprint dimensions and adjusted software measurements was done. The results of these measurements' data plotted relative to each other are given in Figure 7. The relationship between the 62 UAV measurements and blueprint dimensions had a linear trend line with a slope of 1.0069. This means the UAV imagery overpredicts the building dimensions by 0.69%, on average.

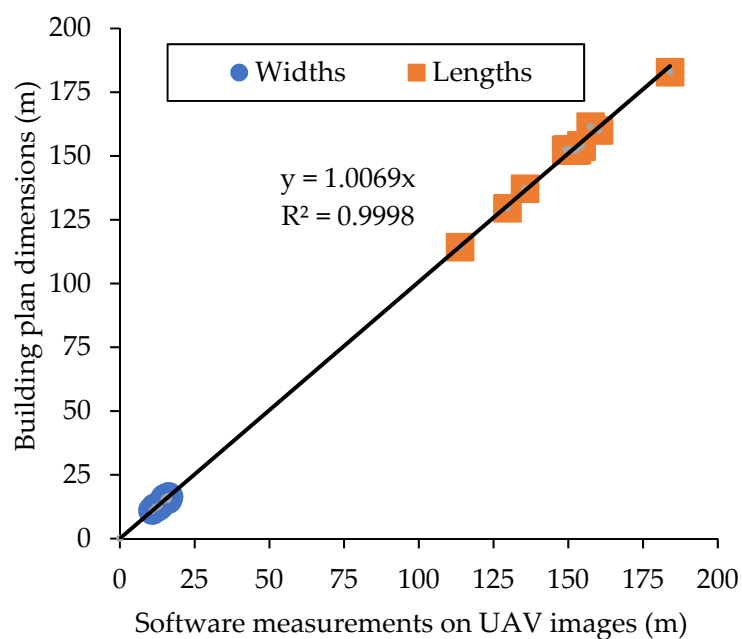


Figure 7. Regression of building length and width measurements between building plan dimensions and UAV software measurements (n = 62).

The results of the calculated differences between the actual measurements (blueprint) and estimated measurements (UAV) for building length and width dimensions are summarized in Table 4. This includes the mean error (Equation (4)), standard deviation, 95% C.I. (Equation (5)), and percent error (Equation (6)). Additionally, an F-test was performed on the length and width error variances, and it was determined that they were significantly different at the 95% C.I. level (the F statistic was 1.61, and the calculated F value was 12.523). Thus, the error measurements were kept separate and not pooled in the summary Table 7. The deviation in poultry house building length is denoted as ΔL and deviation in poultry house building width is denoted as ΔW .

Table 4. Measured error of building width and length between UAV and blueprint plan dimensions.

	ΔW	ΔL
N	31	31
Mean Error (m)	0.0468	1.6621
Standard Deviation (m)	0.3679	1.3021
Variance (m)	0.1354	1.6955
Std. Error of the Mean (m)	0.0661	0.2339
$t_{0.025, 30}$	2.042	2.042
95% CI (m)	± 0.135	± 0.478
Blueprint Grand Mean (m)	14.7681	151.5643
UAV Grand Mean (m)	14.7213	149.9022
Mean Percent Error (%)	0.32	1.10

The mean error for building width measurements was 0.0468 ± 0.135 m. Building widths could be accurately measured in the digital orthomosaics to within 0.32%. The mean error for building length measurements was 1.6621 ± 0.478 m. Building lengths could accurately be measured in the digital orthomosaics to within 1.10%. Both measurement errors' confidence intervals encompassed zero, meaning UAV measurement error was not significantly different from zero at the 95% level.

3.2.2. Poultry House Building Height Measurements

Poultry house building height measurements were taken in the field at 38 instances. These same building dimensions were taken in the UAV-derived DSM at 38 instances for paired comparisons. Poultry building sidewall, side entrance, and peak height measurements ranged from 1.86 to 5.61 m. The results of a regression analysis of the building height hand and software measurements are given in Figure 8.

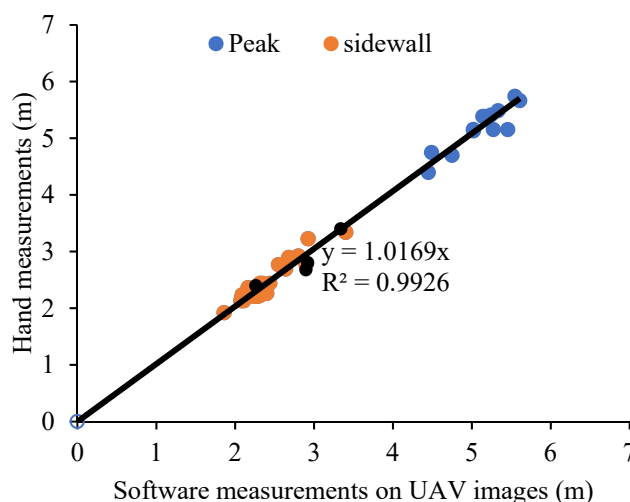


Figure 8. Regression analysis between hand and software measurements of poultry house buildings' side wall, peak, and side entrance heights ($R^2 = 0.99$; $N = 38$).

The relationship between the 38 measurements from UAV images and hand measurements had a linear trendline with a slope of 1.0169. This meant that the UAV imagery overpredicted building heights by 1.69% on average. The results of the differences between actual (hand) and estimated (UAV) measurements for building height dimensions are summarized in Table 5. This includes the mean error (Equation (4)), standard deviation, 95% C.I. (Equation (5)), and percent error (Equation (6)). The deviation in poultry house wall height is denoted as ΔH .

Table 5. Measured error of building heights between UAV and hand measurements.

	ΔH
N	38
Mean Error (m)	0.0617
Standard Deviation (m)	0.1338
Variance (m)	0.0179
Std. Error of the Mean (m)	0.0217
$t_{.025, 37}$	2.026
95% CI (m)	± 0.0440
Hand Measured Grand Mean (m)	3.395
UAV Grand Mean (m)	3.334
Mean Percent Error (%)	1.82

The mean error between the hand and software measured values was 0.062 m. The standard deviation of the software building height measurements was 0.1338 m. The software model measurements had a 95% confidence interval of ± 0.0440 m. A sensitivity analysis was done on the number of trials. A higher number of trials did not return a significantly lower t-value.

3.2.3. Poultry House Rooftop Slope

Rooftop slope was examined for the visited farms using the measured building width and height information as a ratio of height to width using Equation (3). Of the 139 poultry houses visited in the study area, only three houses had a 4:12 slope or 18.4°. All other houses had a 5:12 slope or 22.6°.

3.3. Measured Error from Satellite Imagery

A difference analysis was done on the discrepancy between actual building blueprint dimensions in the horizontal plane and software estimations of poultry house buildings' length and width dimensions. The 31 farms visited had a total 139 buildings. Building length and width measurements were each taken for each in Google Maps [20]. Width measurements ranged from approximately 12 to 20 m, and length measurements ranged from approximately 115 to 188 m. These same measurements were compared with building blueprint dimensions provided by the grower for paired comparisons. The results of a regression analysis of the building lengths and widths between satellite imagery and blueprints are given in Figure 9.

The relationship between the 278 satellite measurements and blueprint measurements had a linear trendline with a slope of 0.9964. This meant that the satellite imagery underpredicted the building footprints by -0.36% on average. The results of the differences between the actual (blueprint) and estimated (satellite) measurements for building length and width dimensions are summarized in Table 6. This includes the mean error (Equation (4)), standard deviation, 95% C.I. (Equation (5)), and percent error (Equation (6)). An F test was performed on the length and width error variances, and it was determined that they were significantly different at the 95% level (the F statistic was 1.35, and the calculated F value was 12.0434). Thus, error measurements were kept separate and not pooled in the summary Table 7. The deviation in poultry house building width is denoted as ΔW . The deviation in poultry house length is denoted as ΔL .

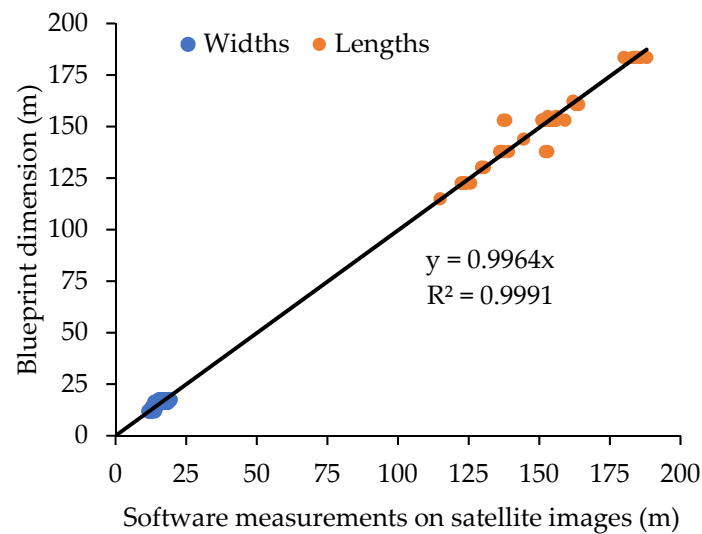


Figure 9. Regression analysis results between blueprint and software poultry house building length and width measurements from satellite imagery (n = 278).

Table 6. Building width and length measured errors between satellite and blueprints.

	ΔW	ΔL
N	139	139
Mean Error (m)	-0.44	-0.45
Standard Deviation (m)	0.8151	2.8286
Variance (m)	0.6644	8.0010
Standard Error (m)	0.0691	0.2399
$t_{0.025,138}$	1.984	2.042
95% C.I. (m)	± 0.1372	± 0.4899
Blueprint Grand Mean (m)	15.62	150.18
Satellite Grand Mean (m)	16.06	150.63
Mean Percent Error (%)	-2.82	-0.30

Table 7. Summary of measured errors between blueprint dimensions and UAV estimations and blueprint dimensions and satellite estimations.

	ΔW	UAV		Satellite	
		ΔL	ΔH	ΔW	ΔL
N	31	31	38	139	139
Mean Error (m)	0.047	1.662	0.062	-0.443	-0.457
95% C.I. (m)	± 0.135	± 0.478	± 0.044	± 0.137	± 0.490

The mean error between the blueprint width measurements and the satellite width measurements was -0.44 ± 0.1372 m. The satellite imagery could accurately predict building blueprint widths to within 2.82%. The mean error between the blueprint length measurements and the satellite length measurements was -0.45 ± 0.4899 m. The satellite imagery could accurately predict building blueprint lengths to within 0.30%.

The results of the statistical analysis of measured error are provided in Table 7. The deviations in poultry house width, length, and wall height are denoted with the symbols ΔW , ΔL , and ΔH , respectively.

The mean error in building width measurements between the blueprint values and UAV width estimations was 0.047 ± 0.135 m ($-0.09, 0.18$). The mean error between the blueprint width and the satellite width estimation was -0.443 ± 0.137 m ($-0.58, -0.31$). The UAV was more accurate, on average, for width estimations with a smaller mean error. Additionally, the average satellite measurement error is below the confidence interval of the UAV estimations. The confidence intervals for the estimation

of the mean do not overlap, meaning the measurement predictions were not in agreement. Lastly, the UAV confidence interval encompassed zero, meaning that there was no significant difference at the 95% level.

The mean error between the blueprint length measurements and the satellite length estimations was -0.457 ± 0.490 m ($-0.95, 0.03$). The mean error for building length measurements between the building blueprints and UAV estimations was 1.662 ± 0.478 m ($1.18, 2.14$). The satellite estimation was more accurate, on average, for length estimations with a smaller mean error. Additionally, the average satellite estimation error is below the confidence interval of the UAV measurements. The confidence intervals for the estimation of the mean do not overlap, meaning the measurement predictions were not in agreement. Additionally, the satellite imagery confidence interval encompassed zero, meaning that there was no significant difference between the satellite estimations and blueprint dimensions at the 95% level.

The rectangular dimensions of the buildings had an average length 10x larger than the building width. The UAV operated at a significantly lower altitude than the satellite while capturing aerial images. This resulted in a reduced field of view for the digital camera and, therefore, an increased image frequency. While building widths were typically captured in 1–3 photos by the UAV, building lengths required 10 to 15 images. If this were expressed as a ratio of image count required to capture building length-to-width, the UAV altitude would dictate a result of 10:1. In contrast, the satellite likely captured an entire building, if not an entire farm, in a single image frame. This would be a length-to-width ratio of 1:1. The increased quantity of images needed by the UAV aerial imaging would explain its larger average error in building length estimations. This lower ratio of images per building dimension may also explain the higher uniformity of error between building length and width estimations from satellite images.

The method that was used to estimate poultry house building dimensions from UAV-captured images can be used for further mapping and analysis. The results proved that a low-cost UAV equipped with an onboard camera can be used for collection of current geospatial data with typical flight path parameters. Estimating rooftop dimensions of poultry houses using UAV imagery provides an alternative approach compared to relatively more expensive LiDAR and manual methods. Although the resolution of UAV images is higher than the publicly available satellite images, for estimating length of rooftops, using UAVs produces a larger mean error than length estimations from satellite images. This would be due to the higher number of images needed to cover the length of the rooftop of a poultry house by a UAV than a satellite image. Estimating the length from multiple images compounding the error producing larger error in length estimations using UAV images than satellite images. If satellite images of the rooftops of a poultry house are not available or not in high quality, an individual can collect aerial images with a UAV and process them in a relatively short time to estimate the length, width, and height dimensions of poultry houses. In addition, the data collection and photogrammetric and geospatial processes can be automated to further increase efficacy and resource allocation. Even the use of a flight path employing vertical image capture (verse oblique) did not compromise the quality of the model's vertical accuracy. These results could further be used for spatial mapping and analysis.

Despite several advantages of UAV aerial imagery, there were a couple of limitations while remotely collecting data. The weather conditions were not always optimal for UAV operation. Occasionally, wind velocity more than 9 m/s would make data collection impossible. Additionally, the Pix4D flight mapper application required mobile cell service to load background maps or that the operator prepare digitally cached base maps of the flight area over a WiFi network in advance. In several instances, base maps could not successfully be loaded in the field due to poor cellular reception in rural areas. The accuracy of the GIS data results was highly sensitive to specific parameters employed during both the remote sensing data collection and the photogrammetry processes. Variations in UAV flight path or photogrammetric tie point limit could significantly impact the final reconstructed output.

4. Conclusions

The results proved that using consumer-grade UAVs and photogrammetric structure from motion (SfM) could create sufficiently accurate digital surface models and orthomosaics for simple building dimension surveys with efficient use of economic and temporal resources while avoiding the use of expensive survey-grade equipment. When compared to the horizontal accuracy of readily available satellite imagery, the results were mixed. The satellite-derived orthomosaics were more accurate, on average, for length estimations, with a smaller mean error. However, the UAV-derived orthomosaic images were more accurate for average width estimations.

The disparity in horizontal measurement accuracy between the remote sensing techniques was likely due to flight altitude and building shape. The rectangular poultry house building dimensions had an average length-to-width ratio of 10:1. The lower flight altitude of the UAV required 10 to 15 pictures to capture building lengths and only 1–3 photos for building widths. In contrast, the satellite field of view likely captured an entire building, if not an entire farm, in a single image frame. This would result in less stitching error in reconstructing building length and may also explain the higher uniformity of error between building length and width measurements from satellite images.

The satellite imagery had a low cost and an ease of access that allowed a convenient determination of structural orientation and planimetric dimensions. However, the UAV provided dependably current data, whereas the temporal accuracy of satellite imagery data was highly variable (sometimes ± 12 months). The UAV-derived data were also useful for determining vertical dimensions and, therefore, variables such as surface slope and aspect. Lastly, the UAV-derived data were more useful for absolute accuracy to establish true object positions in a geodetic coordinate system. This would be critical for analysis of spatial distribution or combining data with GIS data layers from other sources. With an average flight time of 13.5 min per farm area (2.5 ha) and an average ground surface distance of 4.84 cm/pixel, the results obtained from a relatively low-cost UAV equipped with a camera and image analysis demonstrated sufficient accuracy for planning and monitoring purposes of rooftop estimations of poultry houses and possibly other agricultural buildings.

Author Contributions: Conceptualization, J.P.C. and A.B.K.; methodology, P.T.A., J.P.C. and C.P.; software, C.P. and P.T.A.; formal analysis, P.T.A. and J.P.C.; investigation, P.T.A. and J.P.C.; resources, J.P.C.; data curation, P.T.A.; writing—original draft preparation, P.T.A.; writing—review and editing J.P.C. and A.B.K.; project administration, J.P.C. and A.B.K.; funding acquisition, J.P.C. All authors have read and agreed to the published version of the manuscript.

Funding: This research received no external funding.

Acknowledgments: Brian Ritter assisted in photogrammetric and geospatial workflow preparation for data processing. The Clemson University Center for Geospatial Technology provided the software licenses for Agisoft Photoscan Professional.

Conflicts of Interest: The authors declare no conflict of interest. The funders had no role in the design of the study; in the collection, analyses, or interpretation of data; in the writing of the manuscript, or in the decision to publish the results.

References

1. Chastain, J. Opportunities and Challenges Related to Improving Energy Efficiency for Broiler Facilities. In Proceedings of the Momentum: 2016 SEEA & AESP Southeast Conference, Atlanta, GA, USA, 25–26 October 2016.
2. Dennis, C.; Davis, J.; Simpson, G.; Donald, J. *Exploration of Solar Power for the Modern Poultry Farm*. Auburn University Cooperative Extension System; National Poultry Technology Center: Auburn, AL, USA, 2016; pp. 1–6.
3. Lukač, N.; Seme, S.; Žlaus, D.; Štumberger, G.; Žalik, B. Buildings roofs photovoltaic potential assessment based on LiDAR (Light Detection And Ranging) data. *Energy* **2014**, *66*, 598–609. [[CrossRef](#)]
4. Levinson, R.; Akbari, H.; Pomerantz, M.; Gupta, S. Solar access of residential rooftops in four California cities. *Sol. Energy* **2009**, *83*, 2120–2135. [[CrossRef](#)]
5. Verso, A.; Martin, A.; Amador, J.; Dominguez, J. GIS-based method to evaluate the photovoltaic potential in the urban environments: The particular case of Miraflores de la Sierra. *Sol. Energy* **2015**, *117*, 236–245. [[CrossRef](#)]

6. Wiginton, L.K.; Nguyen, H.T.; Pearce, J.M. Quantifying rooftop solar photovoltaic potential for regional renewable energy policy. *Comput. Environ. Urban Syst.* **2010**, *34*, 345–357. [[CrossRef](#)]
7. Lee, S.; Iyengar, S.; Feng, M.; Shenoy, P.J.; Maji, S. DeepRoof: A Data-driven Approach For Solar Potential Estimation Using Roo!op Imagery. In Proceedings of the 25th ACM SIGKDD International Conference on Knowledge Discovery & Data Mining (KDD'19), Anchorage, AK, USA, 4–8 August 2019. [[CrossRef](#)]
8. Kuthanazhi, V.; Jois, S.; Jadhav, P.; Kumar, K.; Magal, A.; Pimpalkhare, A.; Vasi, J.; Kottantharayil, A.; Ramamritham, K.; Narayanan, N.C.; et al. Estimating Mumbai's rooftop PV potential through mobilization of IEEE student community. In Proceedings of the 2016 IEEE 43rd Photovoltaic Specialists Conference (PVSC), Portland, OR, USA, 5–10 June 2016; pp. 3311–3316.
9. Remondino, F.; Barazzetti, L.; Nex, F.; Scaioni, M.; Sarazzi, D. UAV Photogrammetry for mapping and 3D modeling- current status and future perspectives. In Proceedings of the International Archives of the Photogrammetry, Remote Sensing, and Spatial Information Sciences, Zurich, Switzerland, 14–16 September 2011.
10. Hugenholtz, C.; Whitehead, K.; Brown, O.; Barchyn, T.; Moorman, B.; LeClair, A.; Riddell, K.; Hamilton, T. Geomorphological mapping with a small unmanned aircraft system (sUAS): Feature detection and accuracy assessment of a photogrammetrically-derived digital terrain model. *Geomorphology* **2013**, *194*, 16–24. [[CrossRef](#)]
11. Sammartano, G.; Spanò, A. DEM generation based on UAV photogrammetry data in critical areas. In Proceedings of the International Conference on Geographical Information Systems Theory, Applications and Management (GISTAM 2016), Rome, Italy, 26–27 April 2016; pp. 92–98.
12. Uysal, M.; Toprak, A.; Polat, N. DEM generation with UAV photogrammetry and accuracy analysis in Sahitler hill. *Measurement* **2015**, *73*, 539–543. [[CrossRef](#)]
13. Colomina, I.; Molina, P. Unmanned aerial systems for photogrammetry and remote sensing: A review. *ISPRS J. Photogramm. Remote Sens.* **2014**, *92*, 79–97. [[CrossRef](#)]
14. Le Mauff, B.; Juigner, M.; Ba, A.; Robin, M.; Launeau, P.; Fattal, P. Coastal monitoring solutions of the geomorphological response of beach-dune systems using multi-temporal LiDAR datasets. *Geomorphology* **2018**, *304*, 121–140. [[CrossRef](#)]
15. Westoby, M.; Brasington, J.; Glasser, N.; Hambrey, M.; Reynolds, J. 'Structure-from-Motion' photogrammetry: A low-cost, effective tool for geoscience applications. *Geomorphology* **2012**, *179*, 300–314. [[CrossRef](#)]
16. Akturk, E.; Altunel, A. Accuracy assessment of a low-cost UAV derived digital elevation model (DEM) in a highly broken and vegetated terrain. *Meas. J. Int. Meas. Confed.* **2019**, *136*, 382–386. [[CrossRef](#)]
17. Barry, P.; Coakley, R. Accuracy of UAV Photogrammetry Compared with Network RTK GPS. *Int. Arch. Photogramm. Remote Sens.* **2013**, *2*, 2731.
18. AgiSoft PhotoScan. AgiSoft PhotoScan Professional (Version 1.2.6) (Software). 2016. Available online: <http://www.agisoft.com/downloads/installer/> (accessed on 3 April 2020).
19. Ulman, S. The Interpretation of structure from motion. *Proc. R. Soc. B Biol. Sci.* **1979**, *203*, 405–426.
20. Google. Google. In *Google Maps*; Google: Mountain View, CA, USA, 2019.
21. Steel, R.; Torrie, J. *Principles and Procedures of Statistics*; McGraw-Hill Book Company: New York, NY, USA, 1991.
22. Mansurav, N. *EXIF Data Explained*; Photographylife: Englewood, CO, USA, 2020.

Publisher's Note: MDPI stays neutral with regard to jurisdictional claims in published maps and institutional affiliations.



© 2020 by the authors. Licensee MDPI, Basel, Switzerland. This article is an open access article distributed under the terms and conditions of the Creative Commons Attribution (CC BY) license (<http://creativecommons.org/licenses/by/4.0/>).